# Phase Diagram of Tetragonal Manganites

Z. Fang,[1] I. V. Solovyev,[1,2] and K. Terakura[3,4]

[1]*JRCAT-Angstrom Technology Partnership, 1-1-4 Higashi, Tsukuba, Ibaraki 305-0046, Japan*
[2]*Institute of Metal Physics, Russian Academy of Sciences, Ekaterinburg GSP-170, Russia*
[3]*JRCAT-NAIR, 1-1-4 Higashi, Tsukuba, Ibaraki 305-8562, Japan*
[4]*Tsukuba Advanced Computing Center, 1-1-4 Higashi, Tsukuba, Ibaraki 305-8561, Japan*

(Received 24 August 1999)

The phase diagram of $La_{1-x}Sr_xMnO_3$, as a function of hole doping $x$ and tetragonal distortion $c/a$, which consists of ferromagnetic (FM), *A*-, *C*-, and *G*-type antiferromagnetic (AF) states, is obtained by the first-principles band structure calculations. Effects of tetragonal distortion on the magnetic ordering are discussed in terms of orbital ordering and anisotropy in the hopping integrals. The general sequence of the magnetic ground states, FM $\rightarrow$ *A*-AF $\rightarrow$ *C*-AF $\rightarrow$ *G*-AF with increasing of $x$, is also explained based on the instability of FM states with respect to the spin-wave excitations.

PACS numbers: 75.10.Lp, 75.30.Ds, 75.30.Kz, 75.50.Cc

The colossal magnetoresistive (CMR) perovskite manganites $R_{1-x}R'_xMnO_3$ with $R$ and $R'$ being trivalent and divalent ions, respectively (in most cases alkaline-earth or rare-earth elements), have been attracting intense attention over the past few years. They exhibit a remarkably rich variety of structural, magnetic, and transport properties, which can be controlled by various ways: ionic radii of $R$ and $R'$ [1], doping $x$, magnetic field [2], electric field [3], temperature, pressure, and photoexcitation [4]. It is now established that such a unique behavior is due to not only the magnetic degrees of freedom (MDF), but also the orbital degrees of freedom (ODF), and that the MDF and the ODF couples with each other strongly.

The coupling allows one to control the ODF by applying the magnetic field. However, a reverse process is also possible: MDF can be indirectly controlled by the lattice distortion via ODF. Recently Konishi *et al.* [5] succeeded in realizing such control for the CMR manganite $La_{1-x}Sr_xMnO_3$ in the range of $0.3 \leq x \leq 0.5$ by growing thin films on substrates with some different lattice constants. This is a new way of controlling the phases of manganites through the control of $c/a$ ratio. By changing $c/a$ only from 0.97 to 1.06, the phases of $La_{1-x}Sr_xMnO_3$ takes a sequence of the *A*-type antiferromagnetic (AF), the ferromagnetic (FM), and the *C*-type AF states at around $x = 0.5$ [6]. Except the FM state, experimental assignment of the AF orderings (*A*-type, *C*-type, and *G*-type) is indirect and is based on the conjecture by analogy with the well-known system $Nd_{1-x}Sr_xMnO_3$ [7].

The main aim of the present work is to analyze theoretically the phase diagram of tetragonally distorted manganites. We also take $La_{1-x}Sr_xMnO_3$ as an example, because the system can be regarded as the *canonical* CMR manganite. In contrast to other manganites, tilt of $MnO_6$ octahedra in this system is rather small and, as a first approximation, its lattice can be treated as tetragonal. Because of this, an extra complication such as charge ordering does not occur. This enables us to study the fundamental aspects of variations in the magnetic and orbital configurations as functions of the band filling. The present calculation covers the range of doping $x$ from 0.2 to 1.0. To obtain the phase diagram, we adopt the first-principles band structure calculation based on the generalized gradient approximation (GGA) [8,9] in the density functional theory. The pseudopotential method is used and the wave functions are expanded by the plane waves [10]. $La_{1-x}Sr_x$ is treated as a virtual atom by virtual crystal approximation (VCA) [11], whose validity was checked by direct comparison with supercell calculations (SC) [12]. In order to analyze the underlying mechanisms governing the phase diagram, we studied the instability of the FM state by using the frozen spin-wave calculations [13,14].

The phase diagram of Fig. 1(a) is obtained by the total energy analysis, as demonstrated by Fig. 1(b) as an example, which shows total energies for different magnetic

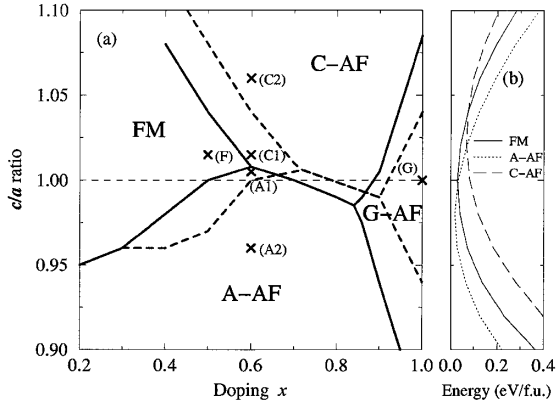


FIG. 1. (a) The phase diagram of $La_{1-x}Sr_xMnO_3$ in the plane of $c/a$ and doping $x$ obtained from total energy calculations as demonstrated in (b). The solid lines give the phase boundaries obtained from calculations with experimental volumes, while the dashed lines correspond to the case with experimental volumes expanded by about 9%. (b) The calculated total energies for different phases of $La_{1-x}Sr_xMnO_3$ as a function of the $c/a$ ratio with fixed doping $x = 0.5$. $c/a$ is varied with the corresponding experimental volume fixed.

  

orderings (FM, *A*-AF, and *C*-AF) as functions of the $c/a$ ratio for the Sr concentration $x = 0.5$. In this case, the result shows that the *A*-AF state is realized for $c/a < 0.99$, the FM state for $0.99 < c/a < 1.04$, and the *C*-AF state for $c/a > 1.04$.

Figure 1(a) clearly shows a tendency that the tetragonal distortion of $c/a > 1.0$ ($c/a < 1.0$) stabilizes the *C*-AF (*A*-AF) state. However, as the boundary between the *A*-AF and *C*-AF states is not parallel to the horizontal axis, the general sequence of the FM → *A*-AF → *C*-AF → *G*-AF states is observed with increasing $x$. We compare this phase diagram with the available experimental information. In the range of $0.97 < c/a < 1.06$ and $0.3 < x < 0.5$ studied by Konishi *et al.* [5], the theoretical phase diagram agrees quite well with the experimental one. In other words, our theoretical analysis gives strong support to their conjectures. In the higher doping region, recently discovered metallic *C*-AF and *G*-AF states in $Sm_xCa_{1-x}MnO_3$ crystal with $x \sim 0.85$ and $0.85 < x < 1.0$, respectively [15], agree with our phase diagram too.

We briefly discuss implications of those phases. Figure 2 shows the densities of states (DOS) for the FM, *A*-, *C*-, and *G*-type AF states corresponding to the marks (×) denoted as *F*, *A*2, *C*2, and *G* in Fig. 1(a). First we note that only the majority spin states have significant DOS at the Fermi level ($E_F$) for FM, *A*-AF, and *C*-AF states [16]. This is a feature characteristic to "half metal." In the FM state, we can expect three-dimensional metallic conduction only in the majority spin state. On the other hand, in the *A*-AF state, electron conduction may be metallic within each spin sublattice (in the *ab* plane) and insulating across the different sublattice (along the *c* axis). A similar situation is found also for the *C*-AF state. In this case, the electron conduction in the *ab* plane is insulating. Although our band theory suggests metallic conduction along the *c* axis, the real situation may be different: low dimensionality and electron correlation may tend to make the *c*-axis transport insulating. Konishi *et al.* [5] measured the resistivity in the *ab* plane and their results are consistent with the above theory. The *c*-axis transport was not measured because of the use of thin films. The end point *G*-AF state corresponding to the *G* point in Fig. 1(a) is insulating. The DOS in Fig. 2 for *A*-AF and *C*-AF clearly suggests a significant difference between $x^2 - y^2$ and $3z^2 - r^2$ orbitals in the population near $E_F$. We summarize in Fig. 3 the electron density distribution for the energy window of 0.6 eV just below $E_F$ for different magnetic states corresponding to all the marks (×) in Fig. 1(a). In addition to the features related with half-metallicity, the orbital ordering will enhance the anisotropy in the transport for the *A*-AF and *C*-AF states.

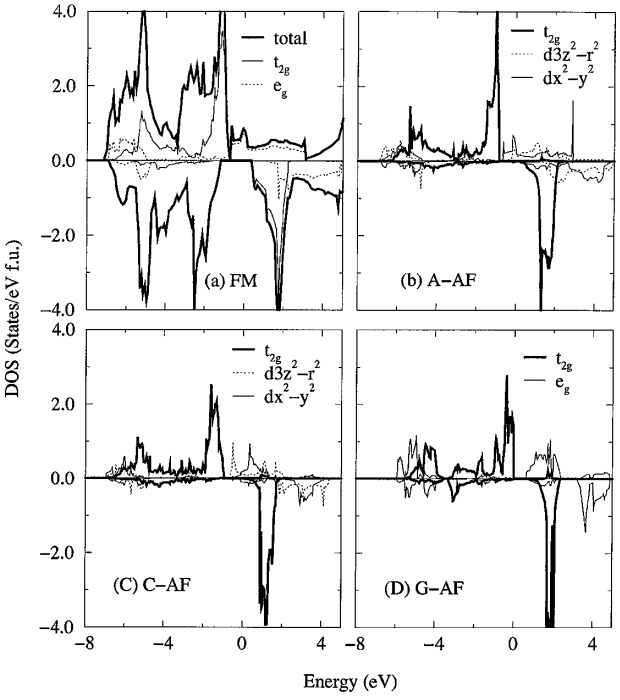


FIG. 2. The total and projected densities of states for (a) FM, (b) *A*-AF, (C) *C*-AF, and (D) *G*-AF states corresponding to the points denoted as *F*, *A*2, *C*2, and *G* in Fig. 1(a). The positive and negative values denote majority and minority spin, respectively. The Fermi levels are located at 0 eV.

In order to understand the phase diagram of Fig. 1(a), we have to consider the correlation among magnetic ordering, orbital ordering, and lattice distortion and also the competition between the double exchange (DE) and the super exchange (SE). Let us first discuss the general tendency caused by tetragonal distortion. We identify two basic mechanisms. The first one is related with the distance dependence of the effective *d*-*d* hopping integral ($t$) and is similar to the band width dependence of the first nearest-neighbor exchange integral $J_1$ discussed in Ref. [17]. $J_1$

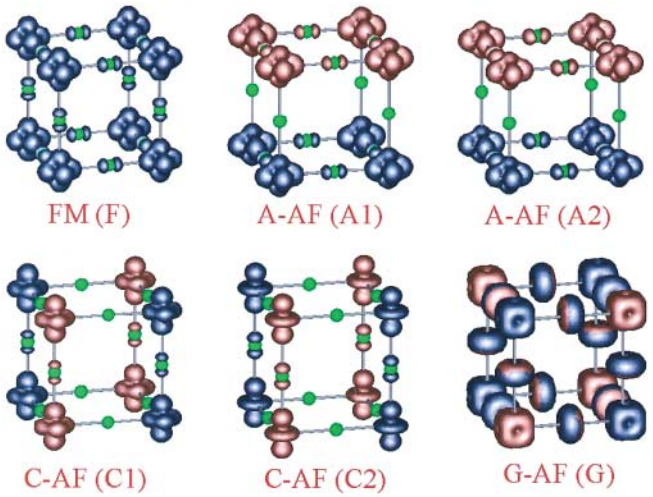


FIG. 3 (color). The calculated charge density distribution for the energy window of 0.6 eV width just below the Fermi level for the different magnetic structures corresponding to all the marks (×) in the phase diagram of Fig. 1. The different spin components (up and down) are drawn as different colors. The Mn atom site at the corners of the cubes, while O atom (green spheres) site at the edge centers.

can be expressed as $J_1 = \alpha t - \beta t^2$ ($\alpha, \beta > 0$) with the first contribution from DE and the second one from SE. The situation realized in the band structure calculations corresponds to the case $2t > \alpha/\beta$, i.e., $\partial J_1/\partial t < 0$. Therefore, as $t$ decreases (increases) when the Mn-Mn distance increases (decreases), $J_1$ is expected to be larger (smaller) in the direction of tetragonal stretching (contraction). This leads to the tendencies towards the *A*-AF and *C*-AF spin orderings for $c/a < 1.0$ and $c/a > 1.0$, respectively. Another more important mechanism is the couping between the MDF and ODF, the latter of which is controlled by the lattice distortion. Since the $e_g$ bands are antibonding states of the O($2p$) and Mn($e_g$) orbitals, the $e_g$ orbital extending along the elongated Mn-O bond will be preferentially occupied when the tetragonal distortion is set in. Accordingly, the $3z^2 - r^2$ orbitals are more populated than the $x^2 - y^2$ ones for $c/a > 1.0$, and vice versa for $c/a < 1.0$. This results in the anisotropy of the FM-DE interactions: For the less than half-filled majority-spin $e_g$ bands, the more (less) populated are the orbitals, the stronger (weaker) are the DE interactions among these orbitals. Such an anisotropy will favor the *A*-AF and *C*-AF spin structures for $c/a < 1.0$ and $c/a > 1.0$, respectively. It should be noted, however, that the orbital polarization and ordering shown in Fig. 3 are related not only with the lattice distortion but also with the magnetic ordering as can be seen in the elctron density distribution corresponding to the points denoted as *F*, *A*1, and *C*1 in Fig. 1(a). $c/a$ is virtually common to these three points, and yet the orbital ordering is quite different among them. Particularly for *A*1, although $c/a > 1.0$, the $x^2 - y^2$ orbital is more populated than the $3z^2 - r^2$ orbital. Anyway, such an orbital polarization is certainly enhanced by tetragonal lattice distortion (*A*1 versus *A*2 and *C*1 versus *C*2). An interesting consequence of orbital ordering and magnetic ordering as realized by lattice distortion is that *electron conduction is suppressed along the direction of lattice compression in contradiction to ordinary cases.*

The increase of $x$ along $c/a = 1.0$ results in the characteristic for three-dimensional manganites sequence of the magnetic ground states: FM $\rightarrow$ *A*-AF $\rightarrow$ *C*-AF $\rightarrow$ *G*-AF. Two theoretical standpoints have been put forward to explain this sequence [18,20]. Below we stress the main differences in the physics between the band structure calculations and these two theoretical models. First, Maezono *et al.* [18] suggested that the driving force behind the change of the magnetic ground states is the on-site Coulomb interaction $U$, which is substantially larger than the one-electron $e_g$ bandwidth $W$, so that the orbital polarization of $e_g$ electrons is nearly complete, giving rise to strong anisotropy of conduction bands, a necessary precondition to stabilize the anisotropic *A*- and *C*-type AF spin structures in the framework of their model. This is certainly very different from the theoretical band approach for manganites [19]. On the other hand, van den Brink and Khomskii [20] argued that DE via degenerate $e_g$ orbitals may be enough to explain the main features of the phase diagram. The DE physics is certainly incorporated in the band approach and is largely responsible for the sequence of the magnetic ground states obtained in the total energy calculations. However, the total picture provided by the band approach is not limited only to the DE physics. The parameters estimated from first-principles band structure calculations typically satisfy the inequality $W/I > 1$ ($I$ being the Hund's rule coupling), which is far from the DE limit. This substantially modifies the frame of magnetic interactions in doped manganites. The analysis of the competition between the FM-DE and the AF-SE originating from $e_g$ bands is given in Ref. [17]. The FM-DE contribution to the first neighbor interactions will be largely compensated by the AF-SE. More importantly, the magnetic interactions become essentially long ranged and can extend far beyond the nearest neighbors. As a result, the FM state in the heavily doped regime becomes unstable with respect to the spin-wave excitations with certain wave vectors. We show the results of the frozen spin-wave calculations [13] for the cubic FM virtual-crystal alloy $La_{1-x}Ba_xMnO_3$ [12,14] in Fig. 4, where locations of the global minima of spin-wave dispersion $\omega(\mathbf{q})$ can tell us not only whether or not the FM state is stable, but also the type of the possible instability. The main directions of this instability have many common features with the phase diagram observed in $La_{1-x}Sr_xMnO_3$. It is important to note that the orbital polarization does not play a role in the present argument.

The validity of our picture can be verified experimentally by an additional way. *The change of the magnetic ground states in the direction FM $\rightarrow$ A-AF $\rightarrow$ C-AF $\rightarrow$ G-AF could also be realized by uniform compression of*

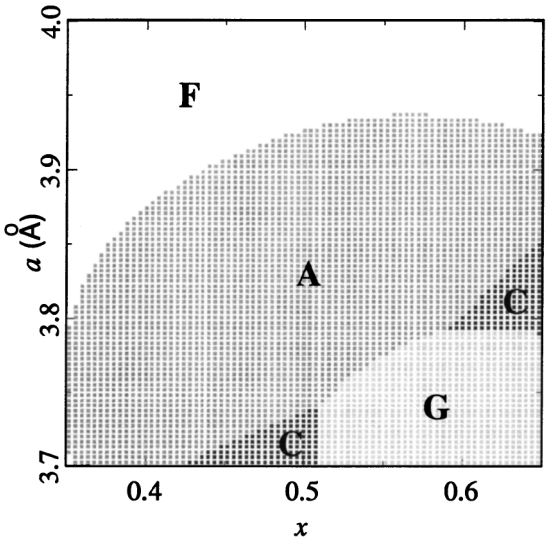


FIG. 4. The points of global minima of the spin-wave dispersion $\omega(\mathbf{q})$. Depending on $x$ and $a$, the FM state can be stable ($F$ area) and unstable with respect to the AF states of *A*-, *C*-, and *G* type.

*the sample*. This is suggested from the study on the effect of volume change on the phase diagram [shown in Fig. 1(a) as dashed line], and also from Fig. 4 more directly.

In summary, we calculated a phase diagram of $La_{1-x}Sr_xMnO_3$ in the plane of $c/a$ and doping $x$, which is well consistent with experimental data. Some implications of the phase diagram were discussed in terms of half metallicity, orbital ordering, and magnetic ordering. The basic mechanism of governing the sequence of magnetic states when tetragonal distortion was set in is assigned to the orbital ordering in ODF induced by lattice distortion which couples with MDF, and the anistropy in the hopping integral induced by tetragonal lattice distortion. It was pointed out that the general sequence of FM $\rightarrow$ *A*-AF $\rightarrow$ *C*-AF $\rightarrow$ *G*-AF with increase of $x$ along $c/a = 1.0$ has close correlation with the instability of FM state towards AF states. We suggest a possible expertimental verification of our picture by uniform compression of the sample.

The authors thank Professor Y. Tokura, Professor M. Kawasaki, Dr. Y. Konishi, and Dr. M. Izumi, for valuable comments and for providing us with their experimental data. The present work is partly supported by NEDO.

[1] See, for example, M. Imada, A. Fujimori, and Y. Tokura, Rev. Mod. Phys. **70**, 1039 (1998).

[2] H. Kuwahara, Y. Tomioka, A. Asamitsu, Y. Moritomo, and Y. Tokura, Science **270**, 961 (1995).

[3] A. Asamitsu, Y. Tomioka, H. Kuwahara, and Y. Tokura, Nature (London) **388**, 50 (1997).

[4] M. Fiebig, K. Miyano, Y. Tomioka, and Y. Tokura, Science **280**, 1925 (1998).

[5] Y. Konishi *et al.*, J. Phys. Soc. Jpn. **68**, 3790 (1999).

[6] The patterns of different AF orderings (*A*-AF, *C*-AF, and *G*-AF) can be seen from Fig. 3 just by the arrangement of colors at the Mn sites (cube corners). *A*-AF is an AF arrangement along the *c* direction of FM layers, while *C*-AF is an AF arrangement of FM chains. *G*-AF is a genuine AF structure.

[7] H. Kuwahara, T. Okuda, Y. Tomioka, A. Asamitsu, and Y. Tokura, Phys. Rev. Lett. **82,** 4316 (1999).

[8] J. P. Perdew, K. Burke, and M. Ernzerhof, Phys. Rev. Lett. **77**, 3865 (1996).

[9] See, for example, H. Sawada, N. Hamada, K. Terakura, and T. Asada, Phys. Rev. B **53**, 12 742 (1996), for the validity of GGA for describing the magnetic states and orbital orderings in transition metal perovskites.

[10] The Mn($3d$) and O($2p$) states are treated by the ultrasoft pseudopotential [D. Vanderbilt, Phys. Rev. B **41**, 7892 (1990)]. The cutoff energy of the plane wave expansion is 30.25 Ry and the number of sampling $k$ points in the irreducible part of the Brillouin zone is 18 for the FM state, and equivalent $k$ points are used for other AF states.

[11] As pseudopotential describes the scattering properties of an atom by treating the valence states as if they are the lowest energy (pseudo) atomic states, the VCA can be applied to alloys consisting of atoms even in different rows of the periodic table. See also J. Lee, J. Yu, and K. Terakura, J. Korean. Phys. Soc. **33,** 55 (1998).

[12] For example, by using the frozen spin-wave method as described below, the first (second) nearest-neighbor magnetic interaction $J_1$ ($J_2$) for $x = 0.25$ at $a = 3.93$ Å, are 30.13 (–2.80) meV in the VCA for $RR' =$ LaBa, 30.44 (–2.81) meV in the SC for $RR' =$ LaBa, and 31.42 (–2.88) meV in the SC for $RR' =$ LaSr. Thus VCA provides a very consistent description for the magnetic interactions.

[13] I. V. Solovyev and K. Terakura, Phys. Rev. B **58**, 15 496 (1999).

[14] These calculations were performed by the all-electron linear-muffin-tin orbital (LMTO) method and Ba was used instead of Sr because of the limitation of the VCA for the all-electron calculations. As the aim of this part of the calculations is to obtain a qualitative insight, the difference between Ba and Sr is not a crucial factor [12].

[15] A. Maignan, C. Martin, F. Damay, B. Raveau, and J. Hejtmanek, Phys. Rev. B **58**, 2758 (1998).

[16] In the *A*-AF and *C*-AF state, the minority spin DOS at $E_F$ is not exactly zero but very small and conduction in this spin channel may be nonmetallic.

[17] I. V. Solovyev and K. Terakura, Phys. Rev. Lett. **82,** 2959 (1999).

[18] R. Maezono, S. Ishihara, and N. Nagaosa, Phys. Rev. B **58**, 11 583 (1998).

[19] Although some orbital polarization effects are inherent to the GGA, they are known to be small for $e_g$ electrons in manganites [H. Sawada, Y. Morikawa, K. Terakura, and N. Hamada, Phys. Rev. B **56**, 12 154 (1997)].

[20] J. van den Brink and D. Khomskii, Phys. Rev. Lett. **82,** 1016 (1999).